International Journal of Hydrogen Energy 61 (2024) 803–819

Contents lists available at ScienceDirect

International Journal of Hydrogen Energy

journal homepage: www.elsevier.com/locate/he

Analysis of the degradation of a Proton Exchange Membrane Fuel Cell for propulsion of a coastal vessel

G. Saponaro, M. Stefanizzi *, M. Torresi, S.M. Camporeale

Department of Mechanics, Mathematics and Management, Polytechnic University of Bari, Via Re David, 200, 70125 Bari, Italy

ARTICLE INFO

Keywords:
PEM Fuel cell
Ferry
Hybrid
Power systems
Fuel cell degradation
Electric propulsion

ABSTRACT

The International Maritime Organization (IMO) is making efforts on reducing pollutant emissions within port areas in order to achieve the ambitious goal of zero net carbon emissions by 2050. This work analyses the effects of the cell degradation on the performance and thermal management of a hydrogen fueled Proton Exchange Membrane Fuel Cell (PEMFC) power system for ferry electric propulsion. The manuscript firstly describes the proposed models, which simulate the fuel cell system and the battery. Then, the development of both an Energy Management strategy and the optimization framework are shown. In details, the zero-order model for the fuel cell and the methodology to estimate its time degradation are described. The accuracy of the model is established through calibration with the characteristic curves of the Ballard FCvelocity™ HD6 PEMFC (150 kW) and further validated against experimental data. The model also involves energy storage and converters that connect both the fuel cell and battery to the electrical grid. The proposed online strategy for the Energy Management System considers four different operating modes and takes into account the estimated fuel cell degradation. Furthermore, the optimization framework finds the solution to achieve the best performance in terms of stack degradation over one year of ship operation, based on a real mission duty cycle. Overall, the efficiency of the fuel cell system decreases by 5%. The degradation involves an increase in fuel consumption of 14.65%. Furthermore, after the last mission, the cooling efficiency achieved through the proposed thermal management strategy is 90%.

1. Introduction

The ferry industry plays an important part in the global transportation landscape, connecting islands to mainlands, even between different Countries. It was estimated that the global ferry industry transported more than 4.3 billion passengers in 2019 [1]. Norway is the first European nation with the largest number of ferries in operation, with 180 ferries employed in 112 routes. The country has taken a world-leading position in electric and hybrid ferries, with plans to have more than 70 fully or hybrid electric vessels by 2022. Ferries play a crucial role in the Norwegian road transport system, connecting communities on islands along the coast. Italy also relies heavily on ferries due to its coastline and numerous islands. The Italian ferry fleet is the second largest in Europe, behind Norway.

Nearly 70% of global GHG emissions occurs within 400 km of coastlines, hence influences the air quality of inhabited coastal areas (about 40% of the world population lives within 100 km of the coastline [2,3]). Then, there is the need to cut down emissions from ships, especially those that operate in coastal waters. According to the classification of the European mandatory Monitoring, Reporting and Verification system (EU-MRV), passenger transport ferries belong to the category of Ro-pax ships. In 2020, this category was responsible for 9.3% of CO_2 emissions from the European maritime transport (level reduced by 21% concerning the emissions in 2019, due to COVID-19 impact [4]).

Electrification of ferries in Italy, along with Greece, Germany, and the UK, would potentially reduce emissions by up to 800,000 tons of CO_2, corresponding to a 50% decrease in the ferry-related emissions in these countries [5]. To enhance the energy transition in ferry transportation, it would be effective to promote the adoption of fully electric ships to replace obsolete vessels on every route up to one hour in duration (long-haul). Furthermore, the average age of European ferry fleet stands at 35 years, with approximately 25% of the ships exceeding 40 years of service, as depicted in Table 1. This involves that over half of the fleet is likely to undergo replacement within this decade [5]. Thus, in order to face legislative constraints, the maritime industry will have to come up with various zero-emissions solutions for new ferries and refit the existing ones.

The electrification of ferries with available technologies such as shore power, hybridization, and electric propulsion for routes of up to

* Corresponding author.
E-mail address: michele.stefanizzi@poliba.it (M. Stefanizzi).

https://doi.org/10.1016/j.ijhydene.2024.02.349
Received 16 December 2023; Received in revised form 22 February 2024; Accepted 27 February 2024
Available online 5 March 2024

Nomenclature

Abbreviations

DC	Direct Current
EMS	Energy Management System
FC	Fuel Cell
GA	Genetic Algorithm
GHG	Green House Gas
HIL	Hardware In the Loop
MEA	Membrane Electrode Assembly
PEM	Proton Exchange Membrane
SOC	State Of Charge

Table 1
Average age of the European ferry.
Source: Data retrieved by [5]

Average age of European ferry fleet	35 years
Share of fleet older than 20 years	64.59%
Share of fleet older than 30 years	44.70%
Share of fleet older than 40 years	25.46%

one hour can significantly contribute to reduce emissions in the ferry industry [5].

Actually, batteries are not feasible to cover medium/long distances, due to the limited storage energy density (referred to the battery mass), around 0.2 kWh/kg depending on type of battery. In comparison, Proton Exchange Membrane Fuel Cells (PEMFC) system shows an energy density of 39.7 kWh/kg (referred to the mass of the FC system) [6]. A more effective and economical approach would be to integrate batteries into hybrid systems, enhancing efficiency by balancing the load with other power sources such as fuel cells or internal combustion engines [7]. Consequently, it is crucial to investigate alternative solutions that offer higher energy storage capacities and recharging or refueling capabilities.

Fig. 1 shows the Ragone plot of the main power generation and energy storage devices. This chart is useful during the preliminary design of the power system, when it is fundamental to identify the most suitable resource that guarantees the reference application demands. Fuel cells appear suitable for those transports that do not require high power density but carry out long-haul routes. This advantage is due to the fact that energy storage is separated from the power generation unit (i.e., the FC itself), ensuring a high density of energy, compared to batteries. The amount of time reported in the Ragone plot represents the time within a device can be operated at its rated power is given as the ratio between the specific energy and the specific power. In a hybrid configuration, fuel cells can provide power for medium-long haul vehicles, allowing the battery to handle peak power demands and energy recovery systems, as shown in [8].

In the past few years, various alternatives to conventional batteries have been developed for powering maritime loads. These alternatives encompass flywheel batteries, renewable energy systems, and hydrogen-based technologies. Hydrogen currently plays a key role for the future global energy landscape because of its carbon-neutral properties. Research in propulsion systems that utilize hydrogen combustion is driving the development of free carbon emissions solutions through the use of gas turbines and direct injection combustion engines [10]. However, hydrogen fuel cell technology appears to be the most suitable for the propulsion and hotel demands of ferry vessels [2,11].

1.1. Literature review

Fuel cells (FC) directly transform chemical energy into electrical energy, avoiding the intermediate conversion into thermal energy typical of combustion engines. This results in reduced NO_x emissions, noise and vibration, while maintaining high levels of efficiency. Thanks to their modular design, fuel cells can be distributed throughout the ship, minimizing electricity transport losses and improving redundancy. FC systems have good part-load performance and a higher volumetric energy density than batteries. Thermodynamic performance by energy and exergy analysis of different fuel cell systems is reviewed in [12], where the parameters influencing the thermodynamic performance of the system are summarized and classified.

The proton exchange membrane fuel cell (PEMFC) has rapidly advanced in recent years, achieving high power densities and improved transient performance. In this case, the fuel cell layers consist of the Proton Exchange Membrane PEM, gas diffusion and catalyst layers. These layers are assembled together and are called the Membrane Electrode Assembly (MEA). A stack with many cells has MEAs positioned between bipolar flow field plates and only one set of end plates. However, the requirement for a wet membrane, while keeping the gas diffusion pores dry, imposes an operating temperature range of 65-85 °C, posing challenges in water management. At lower temperatures, platinum is required to catalyze the electrochemical reaction. In addition, the low operating temperature limits the system tolerance to fuel impurities, particularly carbon monoxide (CO), which is adsorbed from the catalyst surface at these temperatures, deactivating it [13].

The recent scientific literature on Proton Exchange Membrane Fuel Cells (PEMFCs) presents several works with both modeling and experimental approaches.

Different hypotheses and modeling approaches adopted in low computational cost PEMFC system models were reviewed in [14]. In [15] using analytical order reduction and approximation methods, the fluxes and source terms in conventional 1D conservation equations are reduced to six computing nodes at the interfaces between each cell/membrane component. In the work shown in [16,17], two models were developed in the MATLAB-Simulink environment, the first focusing on single-cell modeling, making the model computationally feasible to be integrated into a system-level model, while the second proposes stack modeling and comparison with experimental results.

The high safety risk of hydrogen-fueled systems limits the experimental study of large-scale PEMFC plants, which are rare in the literature compared to configurations between 1–10 kW. Gadducci et al. [18] reported the results of an experimental assessment of a 240 kW real-scale test rig complete with auxiliaries, made up of 8 PEMFC stacks. The experiments focused on the response of the FC system to static, dynamic, and typical maritime operative load profiles. Furthermore, the work gives important suggestions and criteria for the design, construction, and control of similar fuel cell complete systems for maritime applications. Yin et al. [19] described the 5 kW PEMFC laboratory set-up and the related control system. The proposed results concern the improvement of the performance by optimizing the air flow rate at the fuel cell inlet.

The aspect of thermal management was studied by Lim et at. [20] who proposed a methodology for fault diagnosis of the thermal management system to ensure the system reliability by means of an experimental campaign on the thermal management of Low-Temperature PEMFC (LT-PEMFC). Moreover, Oruganti et al. [21] showed the effect of thermal management on the system equipment sizing through simulations. In the work carried out by Hoeflinger et al. [22], a comparison between experimental results and simulations is shown. In this study, the test rig was built starting from a commercially available 30 kW stack and the investigation was focused on the efficiency of the overall system for different ambient and reagents supply conditions.

The degradation of the PEM fuel cells is a critical challenge in their practical applications. Degradation can occur in various components of the fuel cell, including the electrocatalysts for oxygen reduction reaction at the cathode and hydrogen oxidation reaction at the anode. Factors such as fuel/air impurities, harmful species during catalyst preparation and use, and catalyst decomposition during operation contribute to degradation [23]. Environmental conditions (e.g., particularly temperatures below freezing) can also affect the performance and

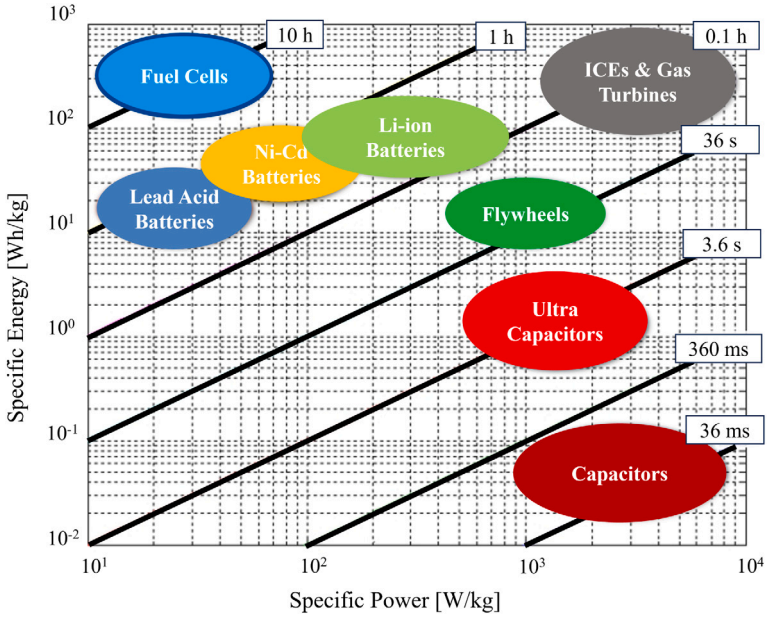

Fig. 1. The Ragone plot of main power generation and energy storage devices.
Source: Data retrieved from [9].

long-term stability of PEMFCs. These causes can lead to changes in the catalyst layers and a reduction of its thickness, ultimately impacting the fuel cell performance. In [24], the authors characterized three different MEAs, estimating performance and degradation for stress cycles between 80 and -10 °C. Fan et al. [25] studied the degradation of the MEA of a PEMFC under Dead-Ended Anode and Cathode (DEAC) operational mode. During this mode of the FC, the generated water cannot be fully removed and then accumulated in the channels, causing a local high voltage to accelerate carbon corrosion or Pt dissolution, thereby influencing the performance of PEMFCs. The diagnosis and prognosis of PEMFCs is discussed in [26], where the main degradation mechanisms (i.e., chemical, electrochemical, and mechanical) and poisoning effects are described. Furthermore, they investigated also the key mitigation strategies.

In the maritime transport sector, PEMFCs can be usefully exploited in ferries, as an alternative to batteries or in combination with them. Wu et al. [2] proposed a holistic design methodology for coastal hybrid ships to optimize its plug-in hybrid fuel cell and battery propulsion system via two case studies. In this work power source degradation and optimal energy management between multiple power sources are considered in the optimization. Aarskog et al. [27] evaluated the economic feasibility of fuel cell powered high speed craft vs. diesel and biodiesel combustion engine solutions. The analysis involves current and a future scenarios, based on real-world operation profiles. FC solution was found to be 28% and 12% more expensive than diesel and biodiesel alternatives, respectively. A sensitivity analysis focusing on seven critical design parameters showed that the most significant factors affecting cost are the hull energy efficiency, the cost of the FC system itself, and the price of hydrogen. In a projected future scenario, between 2025 and 2030, assuming moderate advancements in technology and favorable cost trends, high-speed crafts equipped with FC systems are expected to become cost-competitive with diesel and even more affordable than biodiesel. Letafat et al. [28] investigated the problem of simultaneous optimal energy management and component sizing for a zero-emission ferry ship. A comparison of the proposed configuration in [28] with the existing one also indicates a reduction of the proposed method in reducing the daily operating and investment cost by about 2%. Finally, they suggested a power scheduling, achieved through dynamic programming, 2.4% cheaper than rule-based method. Xie et al. [29] presented a two-level energy management system for a PEMFC/battery hybrid passenger ship to improve the specific fuel consumption during variable cruising conditions. Specifically, the first level is able to customize the power generation plan according to different cruise and FC working conditions. The second level of the EMS is rule-based and it is able to distribute the energy demand. However, in this study FC degradation estimation and prediction are described as future enhancements to enable more practical and accurate operation. In [30], three retrofitting configurations of a Ro-Pax vessel with hydrogen systems were considered for ferries covering the route from Piombino to Elba Island in Italy. Partial retrofitting with the installation of hydrogen FC to power the ship auxiliary systems reduces the overall energy consumption and emissions of the vessel. The study presented in [30] employed an experimental case study to analyze the system configuration and the operation of refueling.

1.2. Research targets

At present, the penetration of PEMFC systems into marine powertrains is limited by the cost of manufacturing fuel cells and the high purity of hydrogen as a fuel. In addition, companies offering PEMFC-based power generation solutions to the marine market must design the product to meet customer requirements, which are different for each application. This significantly increases the cost and resources involved in each project.

The aim of this work is to provide an effective tool for the preliminary design of PEMFC systems that considers the fuel cell in a hybrid configuration, taking into account the interaction with all other equipment on board. The proposed framework, together with the sizing of the FC system, provides important insights into the sizing of the other power system components.

A primary distinction of this research lies in its system design method. This methodology takes into account the interconnections between the fuel cell and other components on the vessel that affect its performance. This extensive level of integration requires a deeper understanding that extends beyond the design of individual parts, emphasizing instead on the synergetic optimization of the whole system. This approach provides an in-depth perspective, ensuring that any proposed feasibility or design solution is not only technically valid, but also practically possible in a real maritime context. The selected case

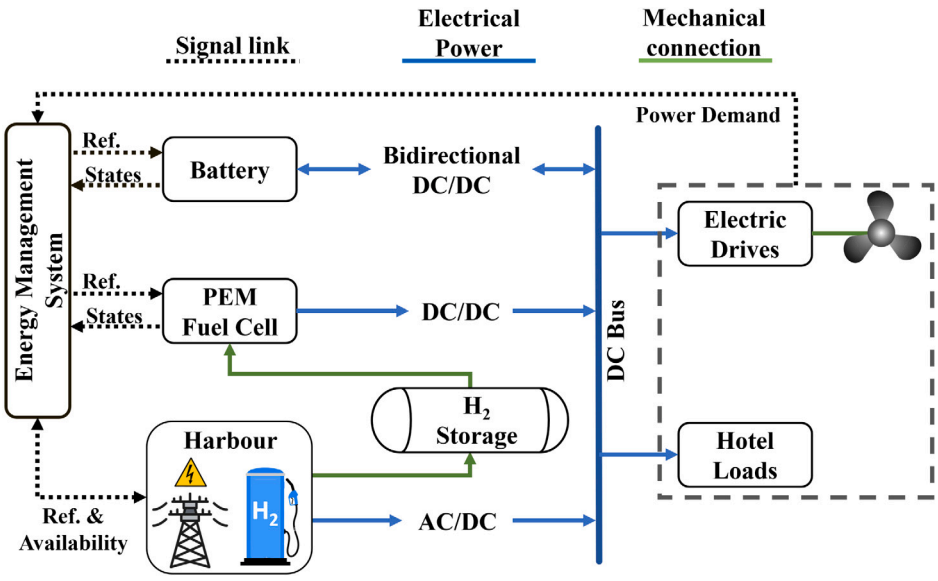

Fig. 2. The schematic of the proposed zero-emission ferry considering the propulsion system, the power generation system and the energy storage.

study concerns a Norwegian ferry, for which data on propulsion power requirements, hotel loads and shore power availability are available.

The presented work studies a power train solution similar to that investigated in [2,28], but extends the analysis by considering a long operating period and the corresponding FC degradation. The proposed online rule-based strategy adapts power scheduling with respect to the estimated cell degradation and the remaining capacity of the energy storage. This solution is currently applicable to actual on-board management systems, simulating the real performance of the generation system. In contrast, the optimal strategy obtained through more complex and computationally demanding methods only finds its application in vessels that have adequate systems to process large amounts of information, such as self-driving vessels.

The simulations assess the feasibility of the hybrid PEMFC power system, taking into account the main issues affecting performance over the years, such as transient performance, FC degradation and thermal management. The optimization framework then finds the solution to achieve the best performance in terms of FC stack degradation over 5000 h of ship operation.

The first part of the work concerns the development of models of PEMFC, auxiliaries and thermal management strategy. After describing the methodology used to model the battery, the EMS and the proposed rule-based strategy are introduced. Afterwards, the optimization framework and its implementation via Matlab GA is presented. Finally, the results obtained for the 600 simulated missions for the configuration with the lowest fuel cell degradation are presented and discussed.

2. The simulation framework

This chapter describes the methodology used to model the different components of the ferry power system. Fig. 2 shows the schematic of the proposed zero-emission ferry. The main power source is the PEM fuel cell system. The battery energy storage operates to obtain a peak shaving of the FC power demand and ensures electrical power to the ship grid allowing the correct dynamic operation of the PEMFC stacks. The online Energy Management Systems (EMS) select the operative mode taking into account the vessel power demand and the battery State Of Charge (SOC) and choose when and how to exploit the power available to the shore (cold-ironing mode). The electrical drives connected to the propellers and the hotel loads represent the power demand of the studied system.

2.1. The fuel cell model

The proposed reduced-order model simulates the FC from an electrochemical and thermodynamic perspective. The model provides also an evaluation of the power absorbed by the oxidizer compressor and auxiliaries. The thermal management strategy applied for the presented PEMFC system is based on the oxidizer stoichiometric excess ratio and the liquid water injected in the oxidizer. The latter is fundamental to ensure the cell membrane humidity. In addition, a degradation estimation model was implemented. Indeed, PEMFCs have a shorter operational lifetime than marine diesel engines due to various factors that can influence the rate of degradation.

The presented PEMFC power system model was developed in the Matlab-Simulink environment. The mathematical model of the single cell and the potential losses (overpotentials) associated with its operation are described, followed by a presentation of the implemented control loop. The proposed model was calibrated on 150 kW Ballard FCvelocity PEM fuel cell available data retrieved from the work presented by Li et al. in 2015 [31].

The model calibration involved a sensitivity analysis in order to evaluate the best values for the customizing variables, as the exchange and limiting current density and the reaction transfer coefficient. Moreover, the test proposed by Li et al. in 2015 was replicated [31] in order to prove the validity of the PEMFC power unit model.

Then, the method used to estimate the fuel cell degradation under different operating conditions is illustrated. The mass and energy balance equations are discussed. Finally, models related to the fuel cell stack and the power required by the auxiliaries are presented.

2.1.1. The single cell model

A fuel cell is an electrochemical cell that converts the chemical energy of a fuel into electricity. Hydrogen is oxidized at the anode and oxygen is reduced at the cathode. Protons are transported from the anode to the cathode through the electrolyte membrane, while electrons travel to the cathode over the external circuit. On the cathode, oxygen reacts with protons and electrons to form water and produce heat. Both electrodes contain a catalyst to speed up the electrochemical processes.

A typical PEM fuel cell operates according to the following reactions, shown in Eqs. (1), (2) and (3):

$$\text{Anode: } H_{2(g)} \rightarrow 2H^{+}_{(aq)} + 2e^{-} \quad (1)$$

$$\text{Cathode: } \frac{1}{2}\,O_{2(g)} + 2H^{+}_{(aq)} + 2e^{-} \rightarrow H_2O_{(g)} \tag{2}$$

$$\text{Overall: } H_{2(g)} + \frac{1}{2}\,O_{2(g)} \rightarrow H_2O_{(g)} + Electric\ Power + Waste\ Heat \tag{3}$$

The key components of a fuel cell are the Proton Exchange Membrane (PEM), the gas diffusion and catalyst layers. These layers are collectively assembled to form what is known as the membrane electrode assembly (MEA). In a fuel cell stack, multiple MEAs are placed between bipolar flow field plates, with just one set of end plates. The maximum energy output of a fuel cell is determined by the change in Gibbs free energy, denoted as ΔG.

Consequently, the theoretical potential of the fuel cell at standard conditions (25° C and 1 atm), E_r^0, is described in Eq. (4), where F is the Faraday's constant and n is the number of electrons involved in the reaction (two in this case). According to Eq. (4), $E_r^0 = 1.229$ V. Eq. (5) is the Nernst equation that can be used in order to compute the FC potential at operating condition different from the standard ones, E_r, as a function of pressure and temperature. ΔS is the entropy variation of the system, T_{op} is the operating temperature of the cell, T_{ref} is the reference temperature equal to 298.15 K, R is the universal elastic gas constant and the partial pressures (p_{H_2}, p_{O_2}, p_{H_2O}) replace the reaction activities of hydrogen and oxygen gases [32].

The potential E_r represents the state when the fuel cell is in open circuit; however, when the circuit is closed, various types of voltage losses occur, each resulting from different phenomena.

$$E_r^0 = \frac{-\Delta G^0}{nF} \tag{4}$$

$$E_r = E_r^0 - \frac{\Delta S}{nF}(T_{op} - T_{ref}) + \frac{RT_{op}}{nF}\ln\left(\frac{p_{H_2}\,p_{O_2}^{0.5}}{p_{H_2O}}\right) \tag{5}$$

As expressed before, there are three kinds of losses (or overpotentials) which make the cell voltage decrease during its operation (i.e. activation, ohmic and concentration overpotentials). The voltage of the single fuel cell V_{cel} is express by Eq. (6).

$$V_{cel} = E_r - V_{act} - V_{ohm} - V_{con} \tag{6}$$

Exceeding the activation energy threshold is essential to initiate a reaction. The activation losses, denoted as V_{act}, reflect the additional energy required beyond equilibrium to start the reaction, predominantly due to electrode kinetics. These losses occur on both the anode and cathode sides.

In a state of equilibrium, the net reaction rate is zero, meaning that forward and reverse reactions proceed at a rate defined by the exchange current density, j_0, a condition known as dynamic equilibrium. When the cell operates at a current density $j > j_0$, the forward reaction predominates, indicative of a completely irreversible reaction process. The relationship between j and j_0 is described by the Butler–Volmer Equation, Eq. (7), as outlined in [27]. In this equation, α represents the transfer coefficient, which indicates how variations in electrical potential across the reaction interface affect the magnitudes of the forward versus reverse activation barriers.

$$j = j_0 e^{\alpha n F(V_{act}/RT_{op})} \tag{7}$$

The value of α is usually between 0 and 1. For symmetric reactions, $\alpha = 0.5$. For most electrochemical reactions, α ranges from about 0.3 to 0.7 [33]. During operating conditions, the fuel cell produces large amounts of net current. This corresponds to an irreversible reaction process where the forward reaction dominates. By solving Eq. (7), we can express the activation overpotential using Eq. (8).

$$V_{act} = \frac{RT_{op}}{\alpha nF}\ln\left(\frac{j}{j_0}\right) \tag{8}$$

Eq. (8) is recognized as the Tafel equation. Initially, this equation was formulated as an empirical rule based on observations in electrochemistry, predating the development of the Butler–Volmer equation. It was not until later that the kinetic theory of Butler–Volmer provided a fundamental explanation for the Tafel equation [32].

The Ohmic losses, denoted as V_{ohm}, are associated with the resistance encountered in the electrolyte to electron flow through the electrically conductive components of the fuel cell, such as bipolar plates and gas diffusion layers, which includes contact resistance. These losses are quantified using Ohm's law in Eq. (9), where R_i represents the equivalent resistance of the fuel cell, and A is the effective surface area of the cell reaction, usually measured in cm^2.

$$V_{ohm} = jAR_i \tag{9}$$

The limiting current density, j_L, in a fuel cell signifies the peak current output that the cell can achieve. This threshold marks the extreme condition for mass transport, occurring when the reactant concentration at the cell surface depletes to zero due to high current density. Nonetheless, concentration losses can occur even at lower current densities. These variations in concentration within the catalyst layer impact the fuel cell efficiency by reducing the Nernst voltage and exacerbating the activation loss. Both these phenomena culminate in what is known as the fuel cell concentration overvoltage, V_{con}, which is calculated using equation Eq. (10) [32,33].

$$V_{con} = \frac{RT}{nF}\left(1 + \frac{1}{\alpha}\right)\ln\left(\frac{j_L}{j_L - j}\right) \tag{10}$$

In order to emulate the real behavior of a fuel cell, V_{con} is often multiplied by an empirical factor in order to improve the results obtained by the cell model at high current densities [32]. For proposed results this gain factor has been set to one. Finally, from Eq. (6) it is possible to obtain the polarization curve that relates the voltage output of the fuel cell for a given current density loading.

The control action, in the developed loop, is the direct current produced by the fuel cell, i. Therefore, the control system is performed by evaluating the error of the actual cell power delivered, P_{cel}, with respect to the reference cell power demand, $P_{d,cel}$. P_{cel} is obtained from the product between the current and the potential given by the polarization curve. The control system analysis was evaluated using the Bode diagram. Table 2 reports the results obtained from the analysis of the Bode diagram.

Table 2
Results from the analysis of the Bode diagram.

Rise time:	2.06 s
Settling time:	3.67 s
Overshoot:	0%
Phase margin:	123° @ 1.98 rad/s
Closed loop stable:	YES

The current, i, and the cell voltage, V_{cel}, are observed during the simulation. Hence, the current output must not exceed the current threshold I_{Lim} and V_{cel} must be between the values $V_{Lim,low}$ and $V_{Lim,up}$. These threshold values can be set by the user according to the datasheet.

2.1.2. The degradation model

The degradation of Proton Exchange Membrane (PEM) fuel cells poses a significant obstacle in their practical applications. This phenomena can affect different parts of the fuel cell, particularly the catalysts. Various elements contribute to this degradation, including impurities in the fuel and air, detrimental substances formed during the manufacturing and operation of the catalysts.

PEMFCs typically have a shorter lifespan compared to marine diesel engines, primarily due to factors like power fluctuations, cycling, and varying load conditions that accelerate their degradation rate. Considering the high manufacturing costs associated with PEMFCs, understanding and accounting for their degradation characteristics is crucial during both the design and operational stages of a ship to ensure cost-effective performance [34].

Table 3
PEM fuel cell degradation rates (per cell) for linear degradation estimation.
Source: Data retrieved by [2,11]

Operating conditions	Deg. rate	Unit
Low power (0%–80% rated power)	10.17	μV/h
High power (80%–100% rated power)	11.74	μV/h
Transient loading	0.0441	μV/ΔkW
Start/stop	23.91	μV/cycle

To accurately determine the rate of voltage degradation under different operational conditions, extensive testing on individual fuel cells is usually required. However, this process can be quite time-intensive. Fortunately, a reliable approximation of this degradation can be derived using data from the manufacturer's datasheet and insights from prior investigations [2,35,36]. The degradation of the cell, denoted as D_{cel}, for a single load cycle can be calculated using Eq. (11).

$$D_{cel} = D_{low} + D_{high} + D_{transient} + D_{cycle} \tag{11}$$

where D_{low}, D_{high}, $D_{transient}$ and D_{cycle} are cell voltage degradation caused by low power operation (less than 80% of the rated power), high power operation, power transient and start/stop cycling, respectively. Table 3 describes the PEMFC single-cell degradation rates used in this study. These parameters may differ across different fuel cell types, depending on the design and actual operating parameters.

The degradation model is executed through a Matlab function, which needs the input of a vector detailing the power output of the cell over time throughout the mission, the sampling time interval, and the rated power of the individual cell.

2.1.3. The stack and auxiliary model

In order to design the whole fuel cell system, including the cooling system, the proposed model not only estimates the performance of the cell from an electrochemical perspective but it also manages the reactant and water flow rates for the thermal balance of the fuel cell. Therefore, the water mass and power balance between the inlet and outlet of the system are evaluated by Eqs. (12) and (13). In Eq. (13), P_{cel} is the electric power output produced by the PEMFC.

For the comprehensive design of the entire fuel cell system, including the cooling system, the proposed model predicts the cell performance electrochemically. It also regulates the flow rates of reactants and water for thermal equilibrium in the fuel cell. Consequently, the water mass and power balance at the system inlet and outlet are calculated using Eqs. (12) and (13). In Eq. (13), P_{cel} represents the electrical power output generated by the PEMFC.

$$\dot{m}^{Ox}_{\mathrm{H_2O},In} + \dot{m}_{\mathrm{H_2O},Inject} + \dot{m}_{\mathrm{H_2O},gen} = \dot{m}^{Ox}_{\mathrm{H_2O},Out} \tag{12}$$

$$\dot{Q}_{H_2,In} + \dot{Q}_{OxIn} + \dot{Q}^{Ox}_{\mathrm{H_2O},In} + \dot{Q}_{\mathrm{H_2O},Inject} = \dot{Q}_{Ox,Out} + \dot{Q}^{Ox}_{\mathrm{H_2O},Out} + P_{cel} \tag{13}$$

The water introduced into the PEMFC, as well as that generated internally, is expelled as vapor in the exhaust, as indicated in Eq. (12). By applying Eq. (12) and (13), it is possible to determine the necessary oxygen stoichiometric ratio and the rate of injected liquid water mass flow rate. This ensures that the exhaust air is fully saturated, eliminating the need for additional cooling or heating of the fuel cell. This approach allows for maintaining the optimal operating temperature while ensuring the correct amount of water at the air outlet to prevent either flooding due to excess liquid water or drying out from overly dry air. In this setup, the relative humidity of hydrogen, which would otherwise humidify the membrane from the anode channels, is disregarded. However, such a fuel cell configuration results in a remarkably straightforward system, as depicted in Fig. 3, which operates without the need for an external water supply for humidification or cooling system.

The presented work does not consider the dynamic on stack humidification. Nevertheless, as described in [37] the humidity regulation at different operating power can optimize the cell dynamic performance. Therefore, the dynamic on stack humidification will be implemented in the proposed model in order to improve the obtained results.

Then it is possible to calculate the flow rate of reactants and the generated water as a function of the current, i, by Eq. (14). $M_{\mathrm{H_2}}$, $M_{\mathrm{O_2}}$ and $M_{\mathrm{H_2O}}$ are the molar weights, whereas the parameters $S_{\mathrm{H_2}}$ and $\mathrm{S_{O_2}}$ are defined as the hydrogen and oxygen stoichiometric ratios, respectively.

$$\begin{cases} \dot{m}_{H_2,In} = \frac{i}{2F} S_{\mathrm{H_2}} M_{\mathrm{H_2}} \\ \dot{m}_{Ox,In} = \frac{i}{4F} \frac{\mathrm{S_{O_2}}}{\chi_{\mathrm{O_2},in}} M_{Ox} \\ \dot{m}_{\mathrm{H_2O},gen} = \frac{i}{2F} M_{\mathrm{H_2O}} \end{cases} \tag{14}$$

The proposed model can simulate PEMFC operation either using pure oxygen or air as oxidizer. Hence, the molar fraction of oxygen, $\chi_{\mathrm{O_2},in}$, could be set as shown in Eq. (15).

$$\chi_{\mathrm{O_2},in} = \begin{cases} 1 & \text{Oxygen as oxidizer} \\ 0.2095 & \text{Air as oxidizer} \end{cases} \tag{15}$$

The calculation of the mass of vapor in the oxidant supplied to the cell and in the exhaust, denoted as $\dot{m}^{Ox}_{\mathrm{H_2O},In}$ and $\dot{m}^{Ox}_{\mathrm{H_2O},Out}$ respectively, is derived from the temperatures of the reactants at the inlet, T_{in}, and the operating temperature, T_{op}. From these temperatures, the corresponding saturated vapor pressure, p_{vs}, is determined. These values, along with the relative humidity of the reactants, φ, are utilized in Eqs. (16) and (17) to ascertain the vapor mass. In these equations, p_{ca} refers to the cathode supply pressure, and p_{out} represents the pressure at the outlet.

$$\dot{m}^{Ox}_{\mathrm{H_2O},In} = \frac{\mathrm{S_{O_2}}}{\chi_{\mathrm{O_2},in}} \frac{M_{\mathrm{H_2O}}}{4F} \frac{\varphi p_{vs}(T_{in})}{p_{ca} - \varphi p_{vs}(T_{in})} i \tag{16}$$

$$\dot{m}^{Ox}_{\mathrm{H_2O},Out} = \frac{\mathrm{S_{O_2}} - \chi_{\mathrm{O_2},in}}{\chi_{\mathrm{O_2},in}} \frac{M_{\mathrm{H_2O}}}{4F} \frac{p_{vs}(T_{op})}{p_{out} - p_{vs}(T_{op})} i \tag{17}$$

As previously mentioned, the model determines the required values for $\mathrm{S_{O_2}}$ and $\dot{m}_{\mathrm{H_2O},Inject}$, essential for maintaining the fuel cell operating state, by resolving Eqs. (12) and (13). The output of hydrogen is contingent upon the set value of $S_{\mathrm{H_2}}$, and the flow rate of the outlet gas is computed using Eq. (18).

$$\dot{m}_{Ox,Out} = \dot{m}_{Ox,In} - \frac{i}{4F} M_{\mathrm{O_2}} \tag{18}$$

Dry air considered components are N_2, O_2, Ar and CO_2. The thermal powers in Eq. (13) are obtained from the product of the flow rate by the standard enthalpy of the species.

The main auxiliary system powered by the PEMFC itself is the system that compresses the oxidizer to operating pressure. The power absorbed by the compressor, P_{com}, for each powered cell is estimated from Eq. (19).

$$P_{com} = \frac{1}{\eta_c \eta_m} \dot{m}_{Ox,In} c_p T \left[\left(\frac{p_{ca}}{p_{amb}} \right)^{\frac{\gamma_a - 1}{\gamma_a}} - 1 \right] \tag{19}$$

Where p_{amb} is the upstream pressure, c_p and γ_a are respectively the oxidizer specific heat and specific heat ratio. η_c is the air compressor efficiency, derived from [38], and η_m is the compressor motor efficiency. The η_c and η_m values, extracted from the technical literature, vary respect to the oxidizer flow rate from zero to the maximum deliverable flow rate. The other auxiliary losses, P_{aux}, are estimated as a percentage of the single-cell gross electrical power produced, P_{cel}, taking into account the fuel cell DC–DC converter efficiency reported in Table 4 extracted from [2].

The stack model introduced requires two key inputs: the number of cells in a single stack, denoted as n_{cel}, and the total number of stacks, n_{stack}, that are linked to the DC bus. In the results presented, each stack is connected directly to the grid. However, the parameter n_{cel} allows for the simulation of connecting multiple stacks in series.

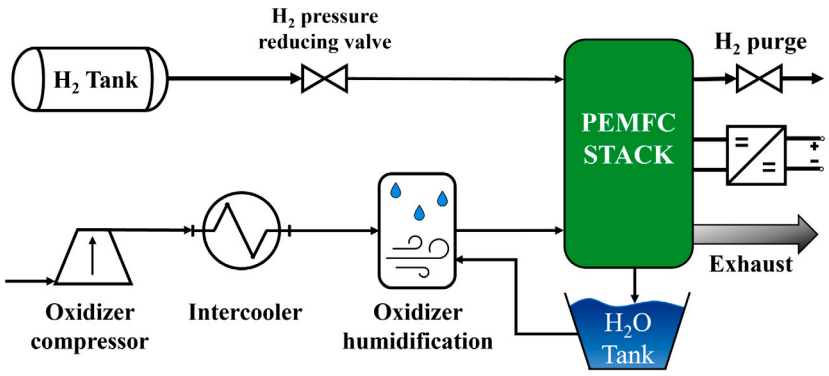

Fig. 3. PEM Fuel Cell proposed system block diagram.

Table 4
PEM fuel cell DC–DC converter efficiency as function of gross power delivered.

Power [$\%_{P_{rated}}$]	Converter Efficiency [%]
10	91.9
20	94.8
30	96.1
40	96.3
50	96.3
60	96.5
70	96.1
80	96.1
90	95.8
100	95.4

The total power requirement for the PEMFC system, referred to as P_{gross}, is calculated using Eq. (20). Here, $P_{mission}$ represents the power needed for shipboard operations, thus defining the net power that is drawn from the power plant.

$$P_{gross} = P_{mission} + (P_{com} + P_{aux}) n_{stack} n_{cel} \tag{20}$$

In addition, the cell power demand, $P_{d,cel}$, is obtained by Eq. (21).

$$P_{d,cel} = \frac{P_{gross}}{n_{stack} n_{cel}} \tag{21}$$

Finally, the overall system efficiency, η_{FC}, is calculated by Eq. (22), considering the system net power $P_{mission}$ and the hydrogen lower heating value (LHV), having gaseous products as exhaust.

$$\eta_{FC} = \frac{P_{mission}}{\dot{m}_{H_2,In}\,\mathrm{LHV}_{H_2}} \tag{22}$$

The thermal management system key parameters are the surplus oxidizer supplied, denoted as S_{O_2}, and the mass of water injected, $\dot{Q}_{H_2O,Inject}$. These parameters are determined based on the operating current of the cell. Consequently, by applying Eq. (23), the efficiency of the proposed thermal management approach, η_{cool}, is assessed over the lifespan of the PEMFC.

$$\eta_{cool} = \frac{\Delta\dot{Q}_{Ox} + \Delta\dot{Q}_{H_2O}}{\dot{Q}_{H_2,In} - P_{cel}} \tag{23}$$

$\Delta\dot{Q}_{Ox}$ and $\Delta\dot{Q}_{H_2O}$ represent the variations in thermal power of the oxidizer and water at the cell inlet and outlet, respectively. These differences indicate the amount of heat being extracted from the system. Additionally, the disparity between the hydrogen heating power, $\dot{Q}_{H_2,In}$, and the electrical power output of the cell, P_{cel}, corresponds to the heat that needs to be dissipated.

2.1.4. Model calibration and validation

The PEMFC selected to power the ferry used as a case study is the FCvelocity™-HD6 manufactured by Ballard. Each stack of this model can generate a maximum power of 150 kW, and the primary operating parameters are detailed in Table 5.

Table 5
PEMFC Ballard FCvelocity™ HD6 operating parameters from technical literature and customizing variables results for calibration on experimental dataset.

Operating parameters		
Cell active surface: A	500	cm^2
Number of cells: n_{cel}	762	
Operating temperature: T_{op}	330	K
Oxidizer	Dry Air	
Anode supply pressure: p_{an}	2.24	bar
Cathode supply pressure: p_{cat}	2.06	bar
Stack max current: I_{Lim}	300	A
Voltage operating range	465 – 730	V
Customizing variables		
Transfer coefficient: α	0.515	
Exchange current density: j_0	1.9E−7	A/cm^2
Limit current density: j_L	0.8	A/cm^2
Average internal resistance: R_i	0.15	$\Omega\ cm^2$
Stack dynamic time constant: τ_{FC}	0.9475	s

To verify the accuracy of the PEMFC power unit model, the test conducted by [31] was performed. Table 5 displays the calibrated values for parameters such as α, j_0, j_L, and R_i, derived from the experimental data on the polarization curve and power output as reported in [31]. The stack dynamic time constant, τ_{FC}, was determined from the analysis of available experimental data, corresponding to the duration required for the system to reach 63% of the power step applied during the test.

Fig. 4 illustrates the outcomes of the model calibration using the experimental data of the fuel cell typical performance. The test investigates the full operational spectrum of the PEMFC up to a current of 300 A, which is the upper limit for the operating current (I_{Lim}).

Following the calibration of the model, a validation test was conducted. This involved simulating the fuel cell transient performance from 14 kW to approximately 140 kW. In detail, the test of the 150 kW PEMFC stack consisted of a load step from 20 A (14 kW — Idle Condition) to 240 A (140 kW). The environmental and stack operating conditions during the test correspond to the parameters used for the calibration listed in Table 5. As shown in Figs. 5 and 6, the reference load step takes 1 s to reach 240 A starting from 20. The simulation used a computing time step of one second, mirroring the approach in the referenced study. The results of the proposed model have been compared with the experimental data in terms of current and electric potential. Specifically, the model is in good agreement with the experimental voltage and current curves, provided in the reference case study.

Fig. 5 depicts a comparison between the outcomes reported by Li Q. et al. [31] and those of the newly developed model, particularly in terms of power output. The figure specifically highlights the dynamic step of the reference power, alongside both the experimental and

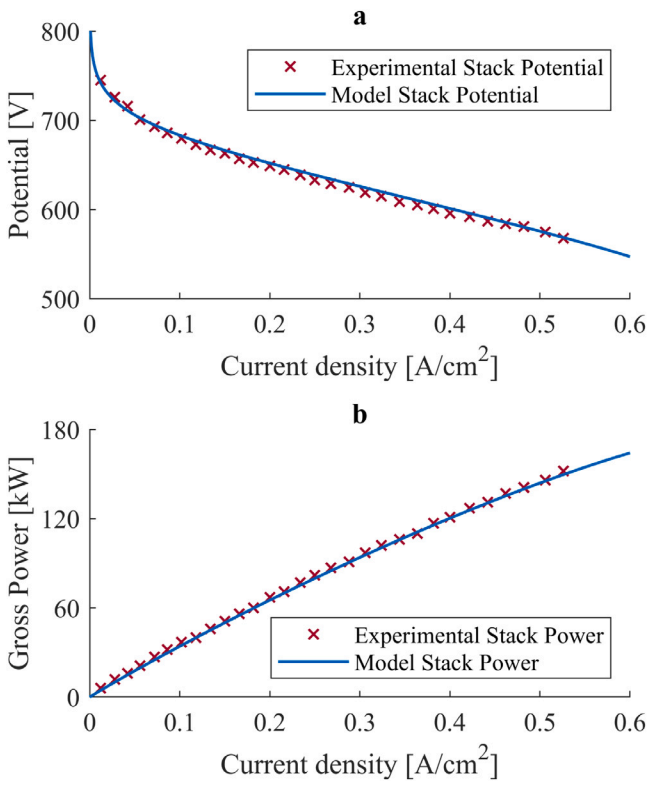

Fig. 4. Comparison between Ballard FCvelocity™ HD6 experimental data and calibrated proposed model. (a) the polarization curve, (b) the power output.

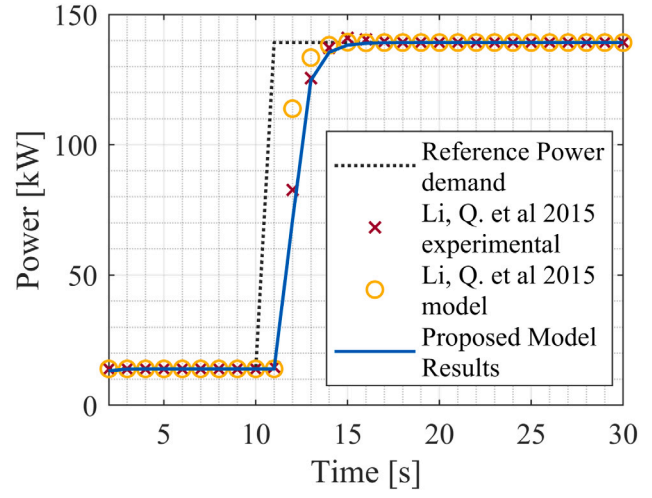

Fig. 5. Comparison between the proposed model (in blue) and experimental (red crosses) and numerical (yellow circles) results proposed by Li et al. [31] in terms of transient power output conditions. (For interpretation of the references to color in this figure legend, the reader is referred to the web version of this article.)

simulation results from [31], and demonstrates the behavior of the model being proposed.

Fig. 6 depicts the results of the validation test in terms of stack current and voltage. The proposed model follows the trend shown by the simulations and experiments carried out in [31], demonstrating the validity and reliability, varying the customizing variables, of the developed model.

2.2. The power system model and management

In this section, the methodology employed to model the power system components external to the fuel cell is presented. In addition, the implementation of the Energy Management System (EMS) and the available operating modes for the case study ferry are discussed.

2.2.1. The energy storage model

Batteries play a crucial role in hybrid ship powertrains. They are used for energy storage and provide power to the propulsive system. The use of lithium-ion batteries is common in these powertrains, as they are the primary battery technology for electric and hybrid vehicles. The implementation of Li-ion batteries in ship power systems has shown potential for reducing CO_2 emissions. Different types of Li-ion batteries, such as lithium titanate and lithium iron phosphate, have been evaluated, with the latter demonstrating better performance. Overall, batteries are an essential component in hybrid ship powertrains, providing efficient and environmentally friendly energy storage and propulsion capabilities. In the presented configuration, the battery is also essential to start-up the fuel cell and to handle the power provided from the harbor grid.

The SOC of the battery represents the Coulombic capacity (Ah) of the storage. Eq. (24) expresses the change of SOC in a time interval dt, where $Q(i)$ is the ampere-hour capacity of the battery at the current rate i.

$$SOC = SOC_0 - \int \frac{i\ dt}{Q(i)} \tag{24}$$

For energy system applications the energy capacity (kWh) is more useful than the coulombic capacity (Ah), because it is directly associated with operations. Eq. (25) defines the energy delivered from the battery, where $V(i, SOC)$ is the actual battery voltage at the defined current rate and SOC.

$$B_c = \int V(i, SOC)\ i(t)\ dt \tag{25}$$

To complete the power generation system model, an energy storage system was integrated. In the model, the battery is considered as an energy storage tank characterized by a capacity, B_c, and a limited charge/discharge rate, C_{rate}. Hence, the battery power output, P_b^{max} is obtained by Eq. (26).

$$P_b^{max} = B_c\ C_{rate}^{max} \tag{26}$$

In this work, the Corvus Orca Energy is taken as default battery, [39]. The capacity of a single battery pack is 124 kWh and the C_{rate} is up to 3 (C_{rate}^{max}). The numerical model takes into account the efficiency of the storage related to the actual State of Charge (SOC), η_b, for a Li-ion battery [40] and the efficiency of the bi-directional DC/DC converter as function of the battery power output (charging/discharging), η_{bc}, taken from [2]. The battery gross power output as function of the net power delivered and remaining capacity is express in Eq. (27).

$$P_{b,Gross} = \frac{P_{b,Net}}{\eta_b\ \eta_{bc}} \tag{27}$$

The Table 6 reports the values of the efficiency of the battery storage cell DC–DC converter for different battery power levels during charging or discharging operations.

2.2.2. The energy management strategy

Integrating the Energy Management System (EMS) is crucial when determining the size of different components. The EMS facilitates the combination of various renewable energy sources and backup systems, addressing the challenges of inconsistent energy supply and guaranteeing uninterrupted power. By optimizing component sizes and implementing an effective energy strategy, the EMS reduces the system total cost and limits adverse impacts.

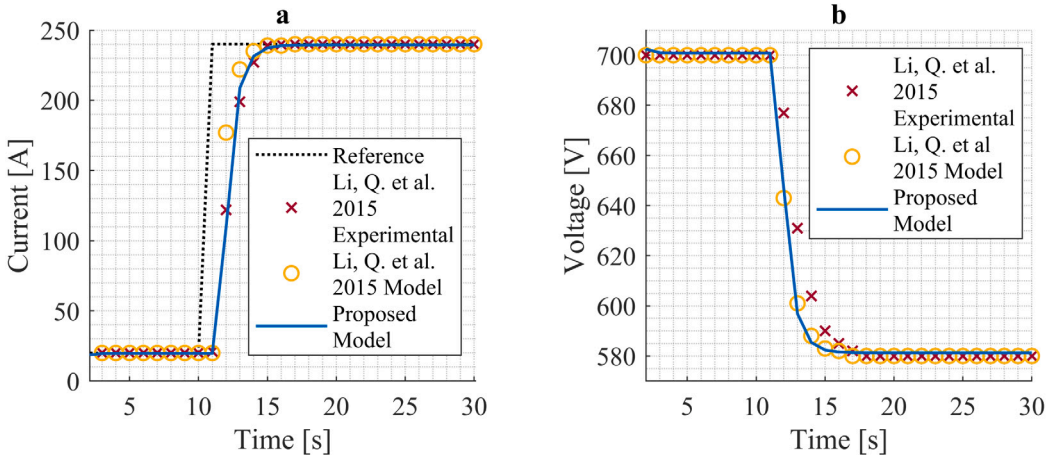

Fig. 6. Comparison between the proposed model (in blue) and experimental (red crosses) and numerical (yellow circles) results proposed by Li et al. [31] in terms of current (a) and voltage (b). (For interpretation of the references to color in this figure legend, the reader is referred to the web version of this article.)

Table 6
Battery storage cell DC–DC converter efficiency as function of gross power delivered.

Power [$\%_{P_{rated}}$]	Converter charging efficiency [%]	Converter discharging efficiency [%]
8.1	88.2	86.3
17.5	92.5	91.4
27.4	94.4	93.8
37.0	95.5	95.0
47.1	96.2	95.7
57.2	96.5	95.9
67.8	96.6	96.2
78.1	96.7	96.2
89.2	97.1	96.3
100	97.0	96.3

The battery energy storage helps to balance out the peak power needs of the Fuel Cell (FC) and provides consistent electrical supply to the ship grid, ensuring the PEMFC stacks function efficiently. The real-time Energy Management Systems (EMS) determines the operating mode based on the ship power needs and the battery state of charge. It also decides when and how to utilize power from the shore during cold-ironing mode.

P_d^{filter} is the total power demand, limited to the maximum PEMFC net power $P_{FC,Net}^{max}$, passed through a low pass filter. The latter is characterized by a customizable time constant τ_{FC} greater than or equal to the stack dynamic time constant. Higher τ_{FC} means lower cut-off frequency which makes the demand power signal smoother. Hence, the P_d^{filter} in Laplace domain (s) can be obtained by Eq. (28).

$$P_d^{filter}(s) = \begin{cases} \dfrac{P_d}{1+\tau_{FC}s}, & \text{if } 0 \le P_d \le P_{FC,Net}^{max} \\ \dfrac{P_{FC,Net}^{max}}{1+\tau_{FC}s}, & \text{if } P_d > P_{FC,Net}^{max} \end{cases} \tag{28}$$

The actual battery state of charge, SOC_{act}, and P_d^{filter} are calculated in the model and used as input for the EMS. Finally, the EMS considers constant values as SOC_M and SOC_m, respectively upper and lower thresholds for the battery capacity, SOC_0, the starting capacity of the storage, and the limit net power output for the PEMFC, $P_{FC,Net}^{max}$, and for the battery, $P_{b,Net}^{max}$. In this work SOC_0 is set to 0.5, SOC_M is 1 and SOC_m is equal to 0.3.

Fig. 7 shows the four states, or modes, that represent the governor of the power generation system and the transition constraints based on the parameters just described. The base state is Default Navigation. In this mode, the power P_d^{filter} is requested to the PEMFC system while the exceeding power demand, positive or negative, is given from the energy storage. Therefore, the exceeding power is positive when the fuel cell delivers more than the power adsorbed by the loads and it is used to charge the battery, when negative is drained from the battery.

During the mission, if the SOC_{act} reaches SOC_M, this condition triggers the "Single Direction Batt". state. This basically works as the "Default Navigation", but the energy storage cannot be charged and it is more exploited until the SOC_{act} returns to SOC_0. If the battery capacity goes lower than SOC_m, "Low SOC Mode" is activated and the fuel cell charges the storage, unless the FC power demand is more than $P_{FC,Net}^{max}$. The last state is the "Cold Ironing", that is activated in case of SOC_{act} lower than SOC_M and the shore power P_{Har} is available. In Cold Ironing, the PEMFC only works for the power requirement that the harbor grid cannot meet, meanwhile the storage is charging. This state remains active until shore power is lacking or the battery is full.

2.3. The optimization framework

Fig. 8 shows the schematic relative to the control of the optimization framework that has been developed. The "Physical Object" represents the existing ferry, which is characterized by its actual power system and operational mission data, such as performance and efficiency. The "Digital Asset" simulates a new layout for the ferry power system using a PEMFC and battery, which must meet the power demands of the "Physical Object". The optimization open variables are the number of PEMFC Ballard FCvelocity™ HD6, N_{FC}, the number of Corvus Orca Energy packs, N_b and the low pass filter time constant, τ_{FC}.

The constraints implemented are presented in Eq. (29), where $P_{Stack,Net}^{max}$ is the limit net power output of a stack of the Ballard FCvelocity™ HD6 and P_{pack}^{max} is the maximum power of the single Corvus Orca Energy pack.

$$\begin{cases} N_{FC}, N_b \text{ are integer} \\ 3 \le N_{FC} \le 15 \\ 1 \le N_b \le 4 \\ 0.947 \le \tau_{FC} \le 50 \\ N_{FC}\ P_{Stack,Net}^{max} + 0.8\ N_b\ P_{pack}^{max} > P_d^{max} \\ N_{FC}\ P_{Stack,Net}^{max} - N_b\ P_{pack}^{max} > 0 \end{cases} \tag{29}$$

The simulation results as power system configuration and performance determine the "Digital Object". The Matlab GA optimization algorithm evaluates the best solution, referred to as the "Optimized Digital Object". The output provided by the proposed optimization recommendations for the sizing and preliminary design of the ferry hybrid power system. The objective function that aims to reduce this work is the PEM fuel cell stack degradation, which is fundamental for all the design aspects, from sizing to evaluating the operational costs.

Table 7 lists the genetic algorithm options selected for this project.

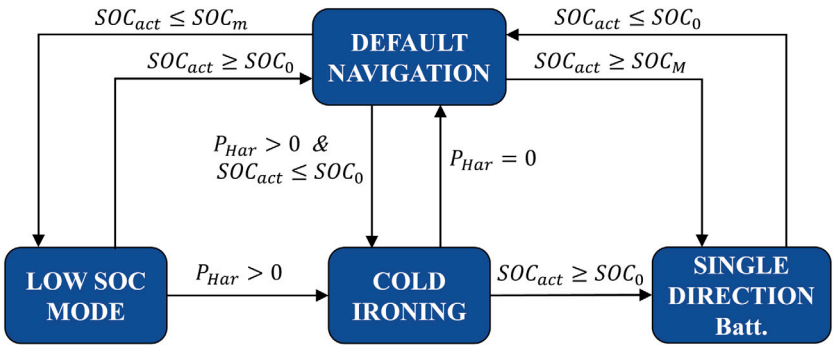

Fig. 7. Energy management strategy navigation modes and transition constraints.

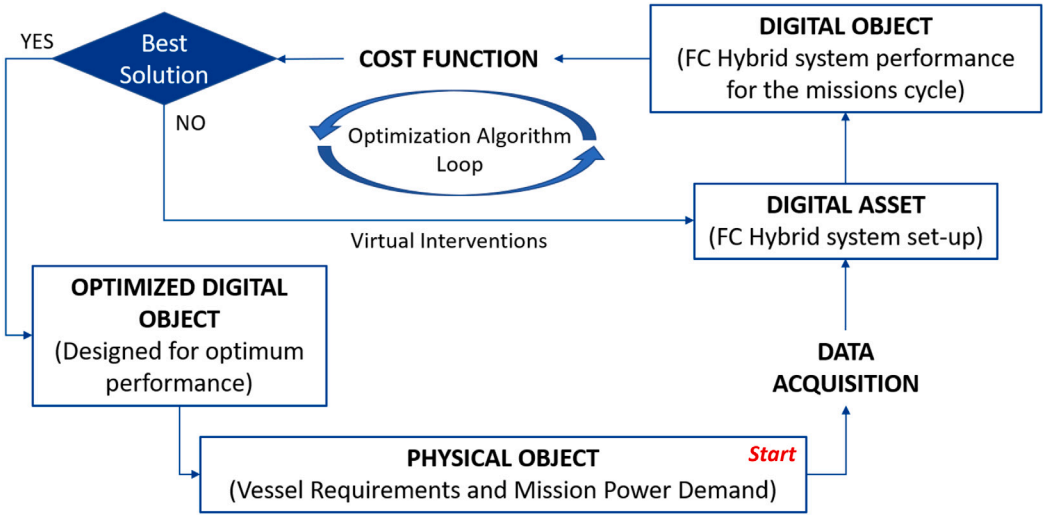

Fig. 8. Schematic of the control applied to the optimization framework.

Table 7
Matlab GA selected options.

Options	Values
Constraints tolerance	1E−3
Crossover fraction	0.2
Elite count	5
Max generations	300

3. The ferry case study

Norway stands out as one of the leading European nations that heavily relies on maritime transport, particularly for covering short to medium distances. This reliance is evident in the fact that a significant portion of its extra-urban mobility is facilitated through ferries. Given its extensive coastline, ferries play an essential role in connecting various regions.

The specific case study selected for this research project is a ferry that sails in Norway. In its current operational setup, this ferry employs a combination of batteries, which serve as its primary source of power, assisted by two diesel generators that act as a backup power source. The onboard electrical infrastructure is based on a direct current (DC) system, and it has been designed to seamlessly integrate with the electrical grid at the port, facilitating easy power exchange. This particular ferry, with its existing configuration, represents an exemplary subject for this research. The presence of a battery-based power system operating within a DC grid offers a unique opportunity. It allows us to conduct a comprehensive feasibility study on the potential integration of a Proton Exchange Membrane Fuel Cell (PEMFC) system. The reliability of this study is further enhanced by the power demand experimental data. Indeed, the power conversion of the case study ferry is the same as the proposed powertrain configuration. This alignment ensures that our findings and recommendations are grounded in real-world operational dynamics, making them both relevant and actionable.

Fig. 9 reports the experimental data corresponding to 8.5 h ferry mission with a sample time of 6 s.

As discussed in the previous section, the case study represents the “physical object”. Thus, all the key data to design and optimize the hybrid PEMFC system are derived from the experimental profiles. The case study was characterized starting from the power demand profiles of the two propulsive electric motors and the ferry hotel load. Moreover, Fig. 9 shows both when the shore power is available and the maximum power of the harbor grid. As can be seen in Fig. 9, the ferry mission is interrupted for 2.5 h after 3.5 h of operation. During the pause, the fuel cell is switched off and only Cold Ironing mode is allowed. This duty cycle has been retrieved by a previous work [41].

The presented model performs the simulation with a time step of one second. The detailed sampling rate of experimental data offers the opportunity to investigate the fuel cell system dynamic performance and to study its coupling capabilities with energy storage such as batteries or supercapacitors. However, the objective of this work is to investigate the feasibility of the PEMFC system to power a long-haul ferry during its entire lifecycle considering the cell degradation rate.

The average target life for a PEM fuel cell system for transports is around 5000 h, as reported in [42,43], so the effects of the degradation on the PEMFC system were studied through the model described above, by simulating a cycle of 600 missions, equivalent to 5100 working hours. At the beginning of each mission, the polarization curve was

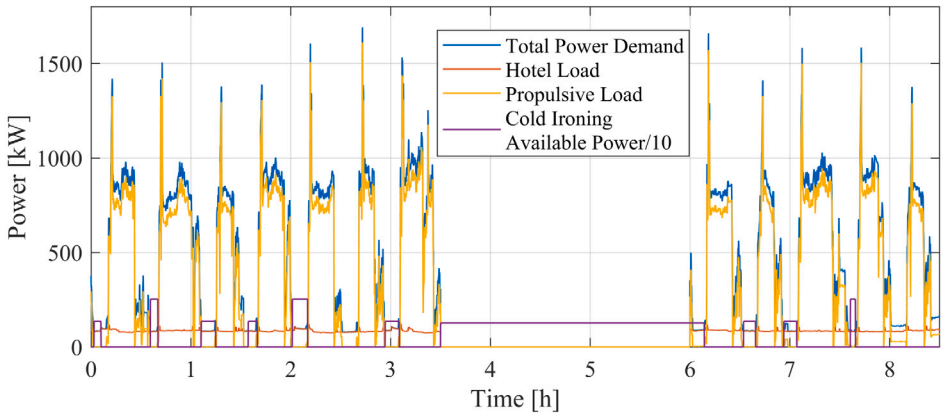

Fig. 9. Mission hotel/propulsive load profiles and the shore power available.

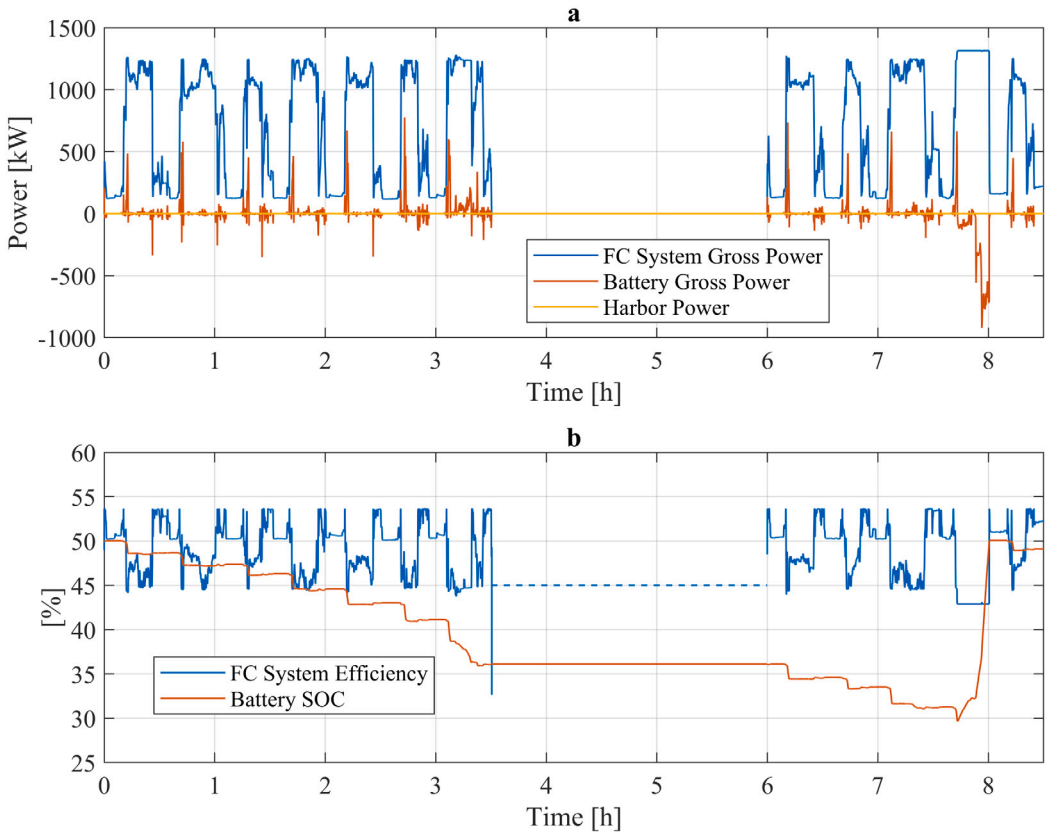

Fig. 10. (a) Mission power profiles of the FC system and battery gross power output and the amount of power taken from the harbor grid; (b) Energy storage capacity and FC system efficiency along the first mission.

updated to take into account the potential lost during the operations. Also $P^{max}_{FC,Net}$ was updated according to the estimated degradation, in order to improve the robustness of the EMS strategy.

4. Results

The optimization algorithm found the best energy source sizing and fuel cell time constant that minimize the stack degradation. The proposed solution consists of 8 PEMFC Ballard FCvelocity™ HD6 (150 kW), 3 Corvus Orca Energy packs (124 kWh per pack) and sets the low pass filter time constant τ_{FC} equal to the natural FC system time constant 0.947 s.

A sensitivity analysis was performed on the effect of τ_{FC} on different feasible plant solutions. For a balanced plant, such as the one obtained from the GA where the battery and fuel cell power ratings are similar, higher values of τ_{FC} are irrelevant or detrimental to stack degradation. Indeed, the PEMFC system had to meet a significantly more stable load than a solution where most of the power is delivered by the fuel cell, and thus higher τ_{FC} values ($>$ 20 s) can have a positive impact on reducing degradation.

The first proposed results are related to the individual mission carried out over 8.5 h, to provide a clear benchmark for assessing the effects of degradation on the system. Fig. 10 shows the power output of the hybrid system, where the negative values of battery power corresponds to storage charging. Moreover, the same figure reports that the EMS chooses not to recharge from the shore grid. Indeed, the bottom part of Fig. 10 shows the trend of SOC_{act}, which ends the mission by storing energy from the FC excess power output and not

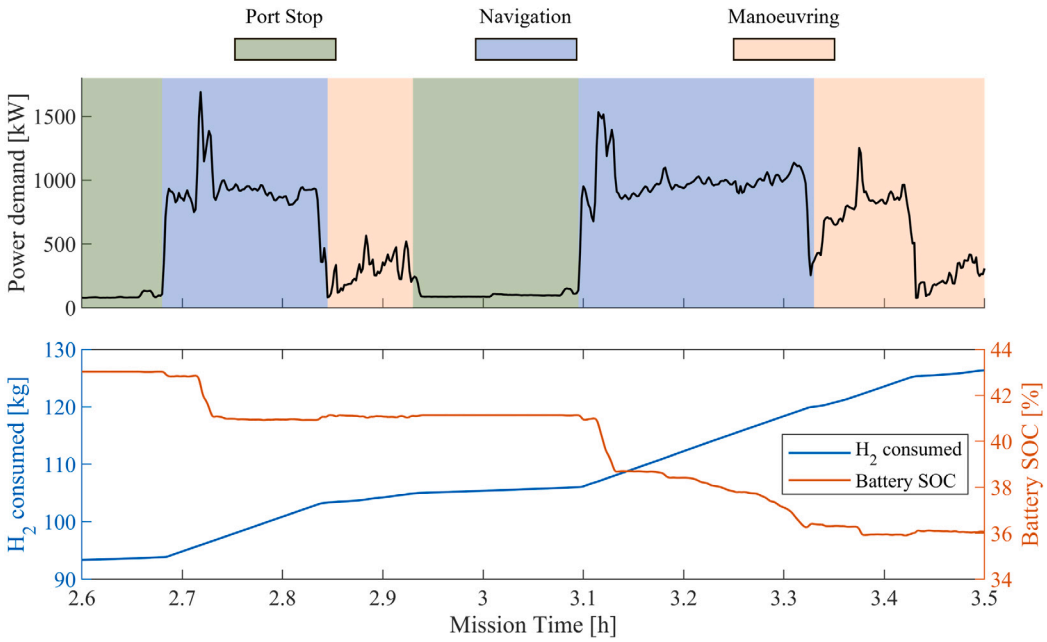

Fig. 11. The power demand and navigation phases, for the mission between 2.6–3.5 h, are described at the top. The trend of consumed hydrogen and battery SOC, during "Default Navigation Mode", are depicted at the bottom.

from the grid. The same picture shows the efficiency of the PEMFC system, which along the mission profile remains stable between 43.7% and 53.7%.

In Fig. 11 part of the first mission is shown in detail, in particular between 2.6-3.5 h, to explain the proposed operation. This route, during the first mission, is traveled in "Default Navigation Mode". The power demand and navigation phases are described at the top: navigation, maneuvering, and stop at the port. At the bottom, the trend of consumed hydrogen and battery SOC are depicted. The rapid increase in power demand, going from stop to sailing and during navigation, is met by using both power resources, where the battery serves the "peak-shaving" function. Energy storage during the other phases is minimally exploited allowing the required load to be coupled with the fuel cell dynamics. During the second sailing period, the power demand exceeds the available power of the fuel cell. In this case, the battery provides power for an extended period while the fuel cell operates at the maximum available load.

Fig. 12 depicts the effect of the degradation on the battery SOC and the PEMFC efficiency during the 600 missions simulation. The efficiency of the fuel cell system never drops under 38.7%. The energy storage capacity trend describes better how the EMS changes its approach to the mission taking into account the potential lost by the FC.

The energy required by the battery increases with the number of missions completed because it must compensate for the loss of FC performance caused by the degradation of the cell. In Fig. 12, it can be seen how depending on the need, the EMS manages battery charging during different port stops.

In Fig. 13 it is evident how, since the 184th mission, the EMS has been using primary system energy and port energy more frequently to recharge the battery. The EMS from mission #393, and even more so from mission #547, mitigates battery utilization, stressing the fuel cell to recharge it. The next progress of this work intends to implement an optimization in order to reduce the overall energy and monetary cost of the period under study.

Fig. 14 provides significant results on the strategy adopted by the EMS during the test cycle showing the percentage of effective navigation time spent in each EMS state.

The "Single Direction Batt." mode was never triggered. Hence in every mission, the battery was able to store the excess power produced by the PEMFC improving its transient performance. Indeed, the "Default Navigation" mode is active most of the time, running both the energy sources in the desired set-up. The PEMFC degradation increases the energy storage exploitation, the reason why the time spent in "Low SOC" Mode and "Cold Ironing" increases after the 300th mission.

The Fig. 15 shows the degradation of the single PEMFC limit potential from the rated value of 730 V to 679 V. The total H_2 consumption for a single mission increases from 198 kg, for the first mission, to the maximum value of 227 kg, during the 575th mission. Therefore, after 4887.5 operative hours, the fuel consumption increases by 14.65%. Obviously, it will be of future interest to analyze the behavior of EMS between mission 500 and 575, where consumption appears very high compared to the trend. Trend resumed in the last mission, after 5100 h of navigation, a consumption of 217 kg of H_2 is recorded, only 9.6% more than the hydrogen consumed during the first mission. The trend of the fuel consumption along the mission cycle gives important insights on the H_2 tank on board, resulting in a more efficient design of the power system and avoiding maintenance costs for the shipowner.

The simulated generation system performed the described mission 600 times in order to evaluate its performance during a total of 5100 operational hours. For each completed mission, it determined the relative degradation and updated the polarization curve for the next mission. As input to the degradation estimation function, the vector of the power produced by the single cell during the concluded mission, as the reference dataset, and the maximum power output of the cell (215 W) were provided.

Fig. 16 shows the polarization curves after several missions conducted, up to #600. The effects of degradation are visible as they reduce the operating voltage of the stack for a given current. Analyzing the polarization curve obtained to perform the 600th mission, it appears that over the entire operating current range (I_{Lim} =300 A) the voltage remains within the range provided by the manufacturer, not dropping below the lower limit of 465 V. The PEMFC system can work properly but delivers less power for the same operating current, as the voltage is decreased.

Fig. 17 describes the trend of the oxidant excess ratio (S_{O_2}) and the amount of water injected in the oxidant gas along the first mission and for all the operative cycles. The excess oxidant never exceeds the value of 4.7, remaining in the range described in the literature [32]. Thus,

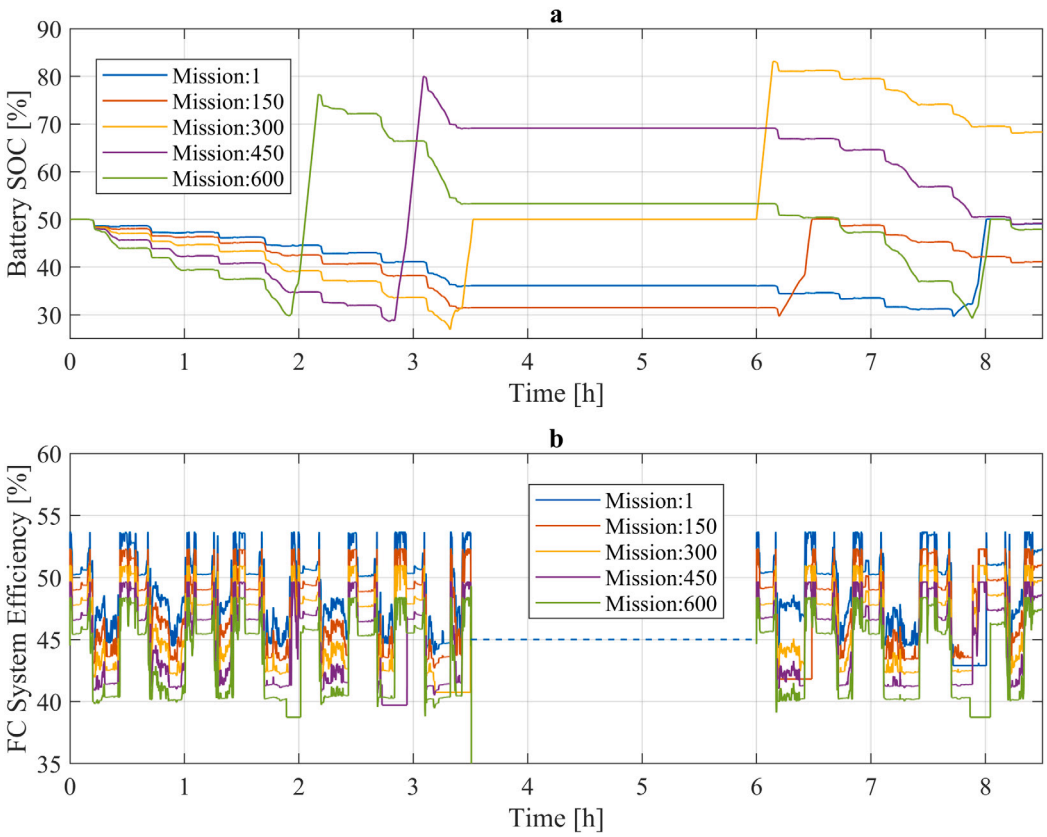

Fig. 12. (a) Effect of degradation on the battery *SOC* along the test simulated; (b) Effect of degradation on the PEMFC efficiency along the test simulated.

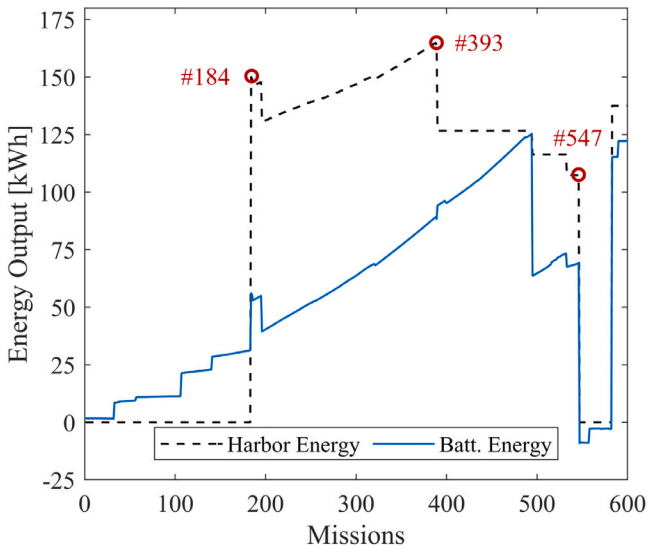

Fig. 13. Total energy provided by the battery and the harbor for each mission.

the proposed strategy turns out to be very effective and easily handled even considering the degradation of FC. The amount of water injected at the oxidant inlet helps to dispose of excess heat and allows the MEA to remain moist.

In conclusion, the results presented show that the designed PEMFC system succeeds in performing the 5100 h of operation before cell degradation making the generation plant unable to supply the required power during the mission.

The last proposed result concerns the average efficiency of the plant thermal management system, illustrated in Fig. 18 as function of the number of missions completed.

The cooling system is designed to dissipate more than 98% of the heat produced during the first mission, but this value drops to about 90% for the last mission. This result confirms the feasibility of the presented PEMFC thermal management strategy, working correctly up to the 600th mission.

5. Conclusions

The maritime industry is facing substantial transformation, primarily driven by the need for sustainable and efficient energy solutions. In this context, the feasibility of integrating a Proton Exchange Membrane Fuel Cell (PEMFC) power system into long-haul ferry operations has been extensively studied.

The degradation estimation of the fuel cell system highlights the operational and sizing critical issues of this technology. Recognizing that system degradation influences hydrogen consumption, energy efficiency, and ultimately operational costs, it becomes evident that the proposed methodology assesses the performance of the system during a long period of operation.

The first result to be discussed concerns fuel cell dynamics. Indeed, the FC system working according to natural dynamics degrades less than the system working with slower dynamics. The fuel cell, when forced to slower dynamics, produces a higher average power that causes it to degrade faster than when working with its natural dynamics (τ_{FC} = 0.947 s). This effect is reduced in solutions where energy is produced almost completely by FC.

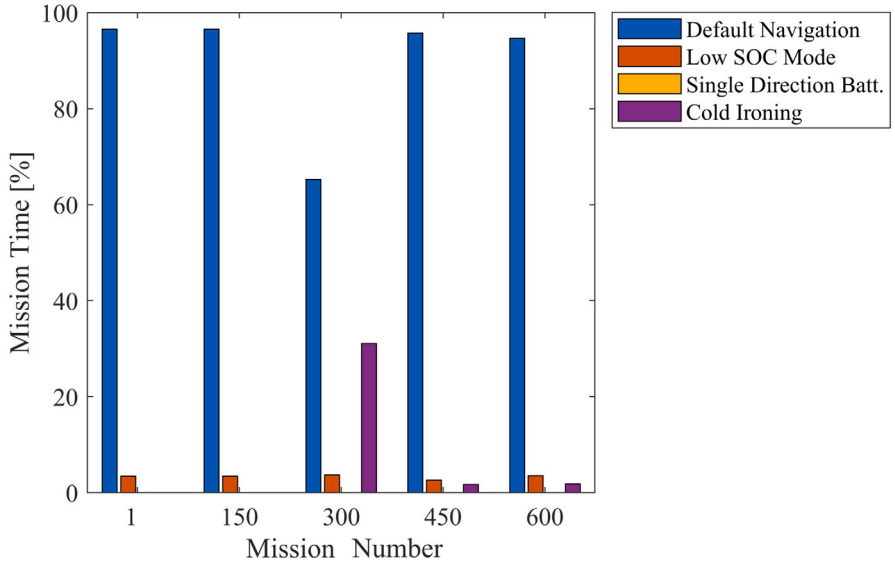

Fig. 14. Effective navigation time for each of the EMS states for five different mission number.

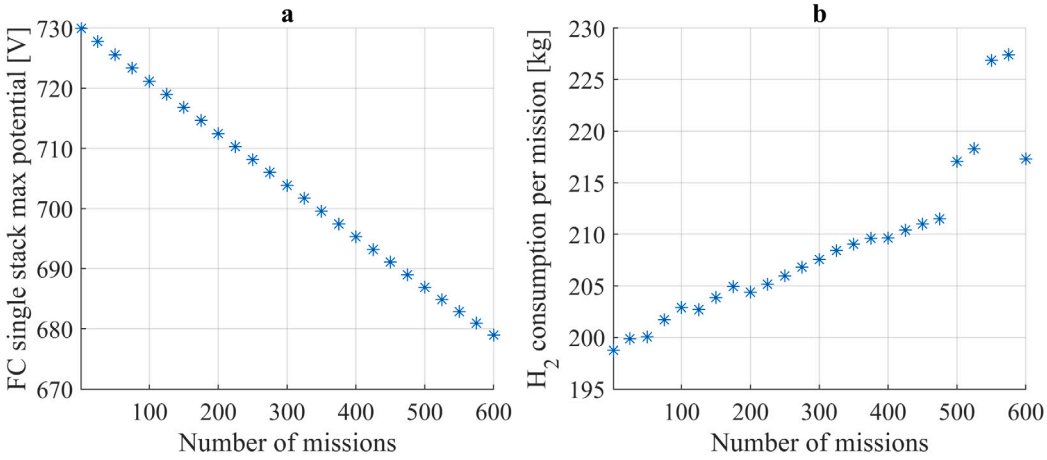

Fig. 15. (a) PEMFC Ballard FCvelocity™ HD6 max potential degradation along the test cycle; (b) Hydrogen consumed per mission along the test cycle.

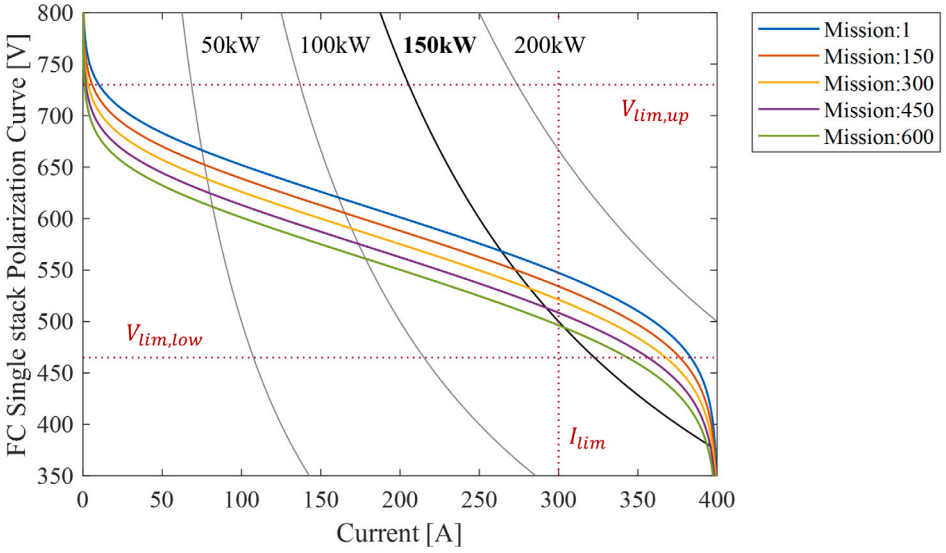

Fig. 16. Single stack polarization curves after the degradation estimated through the proposed linear model.

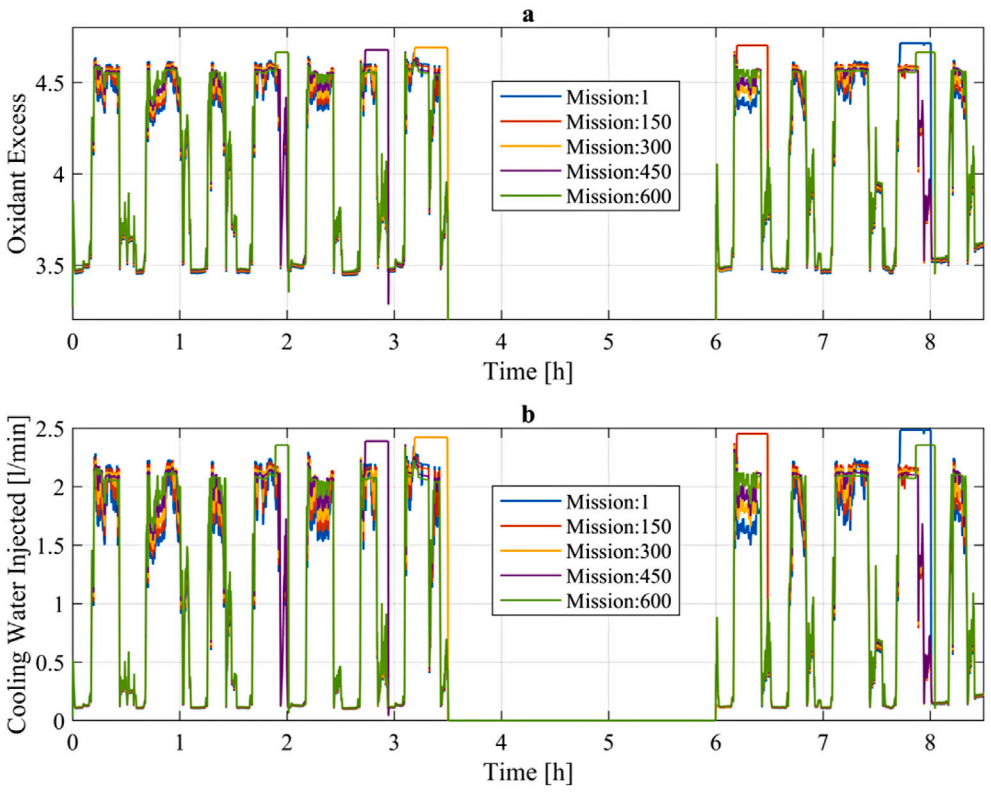

Fig. 17. Trend of the main operating parameters of the thermal management of the single PEMFC stack along the mission cycle. (a) The excess of oxidant required along the missions; (b) The volumetric flow rate of water injected into the oxidant at the inlet.

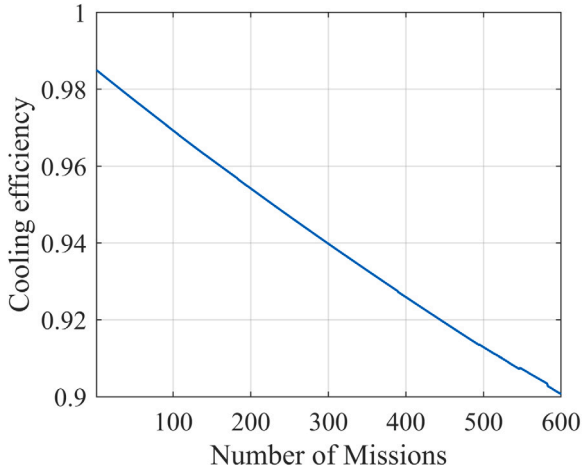

Fig. 18. Trend of thermal management system efficiency along the mission cycle.

The simulation records the performances of the power generation plant and the energy management system for all 600 missions. This means 5100 operational hours, about one year of ferry operational life. The most important insight provided by the analysis is the increase in fuel consumption, which increases by 14.65% during the mission cycle. This result is critical for the sizing of the fuel tank.

The configuration that resulted in the least degradation of the fuel cell is characterized by 8 Ballard stacks (150 kW) and 3 battery packs (124 kWh), with a maximum discharge rate of 3. Thus, 1.2 MW of installed power using FC and approximately 1.1 MW of energy storage. The degraded fuel cell will be able to deliver the same power by working at higher currents, this means more fuel consumption, but also more oxidant flow rate to be delivered by the compressor. The excess oxidant used increased from 3.25 to 3.31 during the analysis. In addition, the average flow rate of injected water, which with air contributes to cell cooling and keeps the membrane moist, increases by 17.6%. Overall, the efficiency of the fuel cell system decreases by 5%. Variations in some parameters are minimal, but this is only due to the proper online energy management strategy adopted, which manages the onboard power sources and port energy.

In conclusion, this research offers valuable insights into the potential and challenges of integrating fuel cell technology in the maritime industry. Employing a holistic approach lays the foundation for future studies that consider the broader implications of technology integration, moving beyond isolated evaluations. As the maritime industry continues its journey toward more sustainable horizons, such comprehensive methodologies will undoubtedly play a pivotal role in its future.

Possible future developments may involve both improvements to the model and experimental implications. The fuel cell model could be improved to provide results regarding the dynamics of the FC membrane cooling and humidification system. The estimation of PEMFC degradation could complement recent advances in the literature. The relevance of this estimation for FC design promoted the experimental study of stress cycles and the study of analytical models to obtain the potential drops due to membrane degradation. An important development in this work concerns synergy with the experimental set-up. Indeed, experimentation on large-scale fuel cell plants, to study the performance of the stack and especially of the cooling system, is essential to obtain more reliable data on which to base simulations. Moreover, the proposed methodology is essential to provide the experimental set-up with the correct insights to study the fuel cell as part of a complex hybrid system in real applications. Hence, integrating this simulation framework into a Hardware In the Loop (HIL) configuration could enable the achievement of important results on the most efficient solutions of integrating the fuel cell system, the future in terms of zero-emission power generation, within marine powertrains, especially those of ferries and other vessels operating on the coastal areas.

Declaration of competing interest

The authors declare that they have no known competing financial interests or personal relationships that could have appeared to influence the work reported in this paper.

Acknowledgments

This work has been supported under the National Recovery and Resilience Plan (NRRP), Mission 4 Component 2 Investment 1.4 - Call for tender No. 3138 of December 16, 2021 of the Italian Ministry of University and Research, funded by the European Union - NextGenerationEU [Award Number: CNMS named MOST, Concession Decree No. 1033 of June 17, 2022, adopted by the Italian Ministry of University and Research, CUP: D93C22000410001, Spoke 14 "Hydrogen and New Fuels"].

References

[1] INTERFERRY. Interferry study reveals ferry industry's huge economic impact. 2021, URL https://interferry.com/2021/10/12/interferry-study-reveals-ferry-industrys-huge-economic-impact/. [Accessed 26 September 2023].

[2] Wu P, Bucknall R. Hybrid fuel cell and battery propulsion system modelling and multi-objective optimisation for a coastal ferry. Int J Hydrogen Energy 2020;45(4):3193–208. http://dx.doi.org/10.1016/j.ijhydene.2019.11.152, URL https://linkinghub.elsevier.com/retrieve/pii/S0360319919343757.

[3] Ayalke ZG, Şişman A, Akpinar K. Shoreline extraction and analyzing the effect of coastal structures on shoreline changing with remote sensing and geographic information system: Case of Samsun, Turkey. Reg Stud Mar Sci 2023;61:102883. http://dx.doi.org/10.1016/j.rsma.2023.102883, URL https://www.sciencedirect.com/science/article/pii/S2352485523000725.

[4] European Commission. Third annual report from the european commission on CO2 emissions from maritime transport. Tech. rep., European Commission; 2022, URL https://climate.ec.europa.eu/system/files/2022-08/swd_2022_214_en_0.pdf.

[5] Siemens. Decarbonizing-marine-transport.pdf. Tech. rep., Siemens; 2022.

[6] Ning F, He X, Shen Y, Jin H, Li Q, Li D, et al. Flexible and lightweight fuel cell with high specific power density. ACS Nano 2017;11(6):5982–91. http://dx.doi.org/10.1021/acsnano.7b01880.

[7] Saponaro G, Stefanizzi M, D'Amato D, Franchini E, Fornarelli F, Torresi M, et al. Modeling and design optimization of a hybrid power generator for full-electric naval propulsion. J Phys: Conf Ser 2022;2385:012087. http://dx.doi.org/10.1088/1742-6596/2385/1/012087.

[8] Cutrignelli F, Saponaro G, Stefanizzi M, Torresi M, Camporeale SM. Study of the effects of regenerative braking system on a hybrid diagnostic train. Energies 2023;16(2). http://dx.doi.org/10.3390/en16020874, URL https://www.mdpi.com/1996-1073/16/2/874.

[9] Moura SJ, Siegel JB, Siegel DJ, Fathy HK, Stefanopoulou AG. Education on vehicle electrification: Battery systems, fuel cells, and hydrogen. In: 2010 IEEE vehicle power and propulsion conference. 2010, p. 1–6. http://dx.doi.org/10.1109/VPPC.2010.5729150.

[10] Stefanizzi M, Capurso T, Filomeno G, Torresi M, Pascazio G. Recent combustion strategies in gas turbines for propulsion and power generation toward a zero-emissions future: Fuels, burners, and combustion techniques. Energies 2021;14(20):6694. http://dx.doi.org/10.3390/en14206694.

[11] Saponaro G, Stefanizzi M, Franchini E, Torresi M, Camporeale S. Modeling and design of a PEM fuel cell system for ferry applications. Tech. rep., SAE Technical Paper; 2023, http://dx.doi.org/10.4271/2023-24-0145.

[12] Nanadegani FS, Sunden B. Review of exergy and energy analysis of fuel cells. Int J Hydrogen Energy 2023;48(84):32875–942. http://dx.doi.org/10.1016/j.ijhydene.2023.05.052, URL https://www.sciencedirect.com/science/article/pii/S0360319923023042.

[13] Van Biert L, Godjevac M, Visser K, Aravind P. A review of fuel cell systems for maritime applications. J Power Sources 2016;327:345–64. http://dx.doi.org/10.1016/j.jpowsour.2016.07.007, URL https://linkinghub.elsevier.com/retrieve/pii/S0378775316308631.

[14] Nóbrega PHA. A review of physics-based low-temperature proton-exchange membrane fuel cell models for system-level water and thermal management studies. J Power Sources 2023;558:232585. http://dx.doi.org/10.1016/j.jpowsour.2022.232585, URL https://www.sciencedirect.com/science/article/pii/S0378775322015622.

[15] Pan Y, Wang H, Brandon NP. A fast two-phase non-isothermal reduced-order model for accelerating PEM fuel cell design development. Int J Hydrogen Energy 2022;47(91):38774–92. http://dx.doi.org/10.1016/j.ijhydene.2022.09.044, URL https://linkinghub.elsevier.com/retrieve/pii/S0360319922041210.

[16] Abdin Z, Webb C, Gray E. PEM fuel cell model and simulation in Matlab–Simulink based on physical parameters. Energy 2016;116:1131–44. http://dx.doi.org/10.1016/j.energy.2016.10.033, URL https://linkinghub.elsevier.com/retrieve/pii/S0360544216314542.

[17] Musio F, Tacchi F, Omati L, Gallo Stampino P, Dotelli G, Limonta S, et al. PEMFC system simulation in MATLAB-Simulink® environment. Int J Hydrogen Energy 2011;36(13):8045–52. http://dx.doi.org/10.1016/j.ijhydene.2011.01.093, URL https://linkinghub.elsevier.com/retrieve/pii/S0360319911001388.

[18] Gadducci E, Lamberti T, Rivarolo M, Magistri L. Experimental campaign and assessment of a complete 240-kW Proton Exchange Membrane Fuel Cell power system for maritime applications. Int J Hydrogen Energy 2022;47(53):22545–58. http://dx.doi.org/10.1016/j.ijhydene.2022.05.061, URL https://www.sciencedirect.com/science/article/pii/S036031992202078X.

[19] Yin L, Li Q, Chen W, Wang T, Liu H. Experimental analysis of optimal performance for a 5 kW PEMFC system. Int J Hydrogen Energy 2019;44(11):5499–506. http://dx.doi.org/10.1016/j.ijhydene.2018.08.157, URL https://www.sciencedirect.com/science/article/pii/S0360319918327320.

[20] Lim IS, Park JY, Choi EJ, Kim MS. Efficient fault diagnosis method of PEMFC thermal management system for various current densities. Int J Hydrogen Energy 2021;46(2):2543–54. http://dx.doi.org/10.1016/j.ijhydene.2020.10.085, URL https://linkinghub.elsevier.com/retrieve/pii/S0360319920338878.

[21] Oruganti PS, Ahmed Q, Jung D. Effects of thermal and auxiliary dynamics on a fuel cell based range extender. In: WCX world congress experience. 2018, p. 2018–01–1311. http://dx.doi.org/10.4271/2018-01-1311, URL https://www.sae.org/content/2018-01-1311/.

[22] Hoeflinger J, Hofmann P. Air mass flow and pressure optimisation of a PEM fuel cell range extender system. Int J Hydrogen Energy 2020;45(53):29246–58. http://dx.doi.org/10.1016/j.ijhydene.2020.07.176, URL https://linkinghub.elsevier.com/retrieve/pii/S0360319920327841.

[23] Yue M, Li Z, Roche R, Jemei S, Zerhouni N. Degradation identification and prognostics of proton exchange membrane fuel cell under dynamic load. Control Eng Pract 2022;118:104959. http://dx.doi.org/10.1016/j.conengprac.2021.104959, URL https://www.sciencedirect.com/science/article/pii/S0967066121002367.

[24] Sabawa JP, Bandarenka AS. Investigation of degradation mechanisms in PEM fuel cells caused by low-temperature cycles. Int J Hydrogen Energy 2021;46(29):15951–64. http://dx.doi.org/10.1016/j.ijhydene.2021.02.088, URL https://www.sciencedirect.com/science/article/pii/S0360319921005917.

[25] Fan L, Zhao J, Luo X, Tu Z. Comparison of the performance and degradation mechanism of PEMFC with Pt/C and Pt black catalyst. Int J Hydrogen Energy 2022;47(8):5418–28. http://dx.doi.org/10.1016/j.ijhydene.2021.11.135, URL https://www.sciencedirect.com/science/article/pii/S0360319921045225.

[26] Wallnöfer-Ogris E, Poimer F, Köll R, Macherhammer M-G, Trattner A. Main degradation mechanisms of polymer electrolyte membrane fuel cell stacks – Mechanisms, influencing factors, consequences, and mitigation strategies. Int J Hydrogen Energy 2024;50:1159–82. http://dx.doi.org/10.1016/j.ijhydene.2023.06.215, URL https://www.sciencedirect.com/science/article/pii/S0360319923031683.

[27] Aarskog FG, Danebergs J, Strømgren T, Ulleberg O. Energy and cost analysis of a hydrogen driven high speed passenger ferry. In: Visser K, Baldi F, Van Biert L, editors. Int Shipbuild Prog 2020;67(1):97–123. http://dx.doi.org/10.3233/ISP-190273, URL https://www.medra.org/servlet/aliasResolver?alias=iospress&doi=10.3233/ISP-190273.

[28] Letafat A, Rafiei M, Sheikh M, Afshari-Igder M, Banaei M, Boudjadar J, et al. Simultaneous energy management and optimal components sizing of a zero-emission ferry boat. J Energy Storage 2020;28:101215. http://dx.doi.org/10.1016/j.est.2020.101215, URL https://linkinghub.elsevier.com/retrieve/pii/S2352152X19317177.

[29] Xie P, Asgharian H, Guerrero JM, Vasquez JC, Araya SS, Liso V. A two-layer energy management system for a hybrid electrical passenger ship with multi-PEM fuel cell stack. Int J Hydrogen Energy 2024;50:1005–19. http://dx.doi.org/10.1016/j.ijhydene.2023.09.297, URL https://www.sciencedirect.com/science/article/pii/S0360319923050103.

[30] Melideo D, Desideri U. The use of hydrogen as alternative fuel for ship propulsion: A case study of full and partial retrofitting of roll-on/roll-off vessels for short distance routes. Int J Hydrogen Energy 2024;50:1045–55. http://dx.doi.org/10.1016/j.ijhydene.2023.10.142, URL https://www.sciencedirect.com/science/article/pii/S0360319923052503.

[31] Li Q, Chen W, Liu Z, Li M, Ma L. Development of energy management system based on a power sharing strategy for a fuel cell-battery-supercapacitor hybrid tramway. J Power Sources 2015;279:267–80. http://dx.doi.org/10.1016/j.jpowsour.2014.12.042, URL https://linkinghub.elsevier.com/retrieve/pii/S0378775314020709.

[32] O'Hayre R, Cha S-W. Fuel cell fundamentals. Wiley; 2016, http://dx.doi.org/10.1002/9781119191766.biblio.

[33] Spiegel C. PEM fuel cell modeling and simulation using MATLAB. Elsevier; 2011, http://dx.doi.org/10.1016/B978-0-12-374259-9.X5001-0.

[34] Corda G, Breda S, D'Adamo A. A MATLAB/Simulink model of a PEM fuel cell system including ageing phenomenon. Tech. rep., SAE Technical Paper; 2023, http://dx.doi.org/10.4271/2023-24-0148.

[35] Chen H, Pei P, Song M. Lifetime prediction and the economic lifetime of Proton Exchange Membrane fuel cells. Appl Energy 2015;142:154–63. http://dx.doi.org/10.1016/j.apenergy.2014.12.062, URL https://linkinghub.elsevier.com/retrieve/pii/S0306261914013191.

[36] Fletcher T, Thring R, Watkinson M. An Energy Management Strategy to concurrently optimise fuel consumption & PEM fuel cell lifetime in a hybrid vehicle. Int J Hydrogen Energy 2016;41(46):21503–15. http://dx.doi.org/10.1016/j.ijhydene.2016.08.157, URL https://linkinghub.elsevier.com/retrieve/pii/S0360319916325435.

[37] Fang M, Wan X, Zou J. Development of a fuel cell humidification system and dynamic control of humidity. Int J Energy Res 2022;46(15):22421–38. http://dx.doi.org/10.1002/er.8547.

[38] Nelson SA, Filipi ZS, Assanis DN. The use of neural nets for matching fixed or variable geometry compressors with diesel engines. J Eng Gas Turbines Power 2003;125(2):572–9. http://dx.doi.org/10.1115/1.1563239, URL https://asmedigitalcollection.asme.org/gasturbinespower/article/125/2/572/447136/The-Use-of-Neural-Nets-for-Matching-Fixed-or.

[39] Corvus orca ESS. 2023, https://corvusenergy.com/products/energy-storage-solutions/corvus-orca-energy/. [Accessed 22 November 2023].

[40] Vepa R. Dynamic modeling, simulation and control of energy generation. vol. 20, Springer; 2013.

[41] Saponaro G, D'Amato D, Stefanizzi M, Franchini E, Osen O, Hasan A, et al. Fuel-cell hybrid power system preliminary design optimization for ferry application. In: 2023 IEEE energy conversion congress and exposition. Vol. 2385, IEEE; 2023, p. 6389–96. http://dx.doi.org/10.1109/ECCE53617.2023.10362942.

[42] Capurso T, Stefanizzi M, Torresi M, Camporeale S. Perspective of the role of hydrogen in the 21st century energy transition. Energy Convers Manage 2022;251:114898. http://dx.doi.org/10.1016/j.enconman.2021.114898, URL https://linkinghub.elsevier.com/retrieve/pii/S0196890421010748.

[43] Glosten I. Ferry fuel & propulsion feasibility study final report. Tech. Rep., NYC Department of Transportation; 2022.